Journal of Structural Geology 32 (2010) 1305–1316

Contents lists available at ScienceDirect

Journal of Structural Geology

journal homepage: www.elsevier.com/locate/jsg

Inferred fluid flow through fault damage zones based on the observation of stalactites in carbonate caves

Young-Seog Kim [a,*], David J. Sanderson [b]

[a] Department of Environmental Geosciences, Pukyong National University, Busan 608-737, Republic of Korea
[b] School of Civil Engineering and the Environment, University of Southampton, SO17 1BJ, UK

ARTICLE INFO

Article history:
Received 3 December 2007
Received in revised form
5 January 2009
Accepted 9 April 2009
Available online 12 May 2009

Keywords:
Fault damage zones
Fluid flow
Limestone cave
Stalactites
Fractured reservoirs

ABSTRACT

Faults and fractures are important factors that control fluid flow in rock masses in hydrothermal, groundwater, and hydrocarbon systems. In this paper we examine local variations in fluid flow as evidenced by the distribution patterns and sizes of stalactites in fractured limestone. We observe that the size and distribution of stalactites relate to fluid flow and is strongly controlled by the fracture apertures, intersection of fractures, and development of damage zones around a fault.

Fault damage zones are the volumes of deformed wall rocks around a fault surface that result from the initiation, propagation, interaction, termination, and build-up of slip along the fault. They are divided into tip-, wall-, and linkage damage zones depending on their location along the fault. The pattern of deformation within a damage zone mainly depends on fault tip modes (mode II or III), the 3-D locations around a fault surface, and the evolutionary stage of the fault. The development of different structures within damage zones gives valuable information about fault initiation and termination, fault propagation and growth, and fluid flow.

Stalactites indicate fluid flow variation within a fault in that fluid flow is high in dilational jogs, variable along the main fault traces, and low in contractional jogs. Variation in ore fluid flow within faults is also important in controlling the position of ore shoots in structurally-controlled hydrothermal mineral deposits. Thus, the characteristics of fluid flow in fractured carbonate rocks can be related to patterns of damage around faults. Hence, the mapping of damage zones can be applied to the study of fracture-controlled fluid flow in the fields of petroleum geology, hydrogeology, and ore deposits.

1. Introduction

Faults and fractures are important in controlling fluid flow in many groundwater and hydrocarbon reservoirs. The specific reaction of the reservoirs to deformation depends on the amount and direction of displacement, the response of wall rocks, and the nature of the rock in the fault zone. Simple fractures (or joints) can influence the porosity and permeability of the rock. The opening of fractures due to deformation leads to both enhancement and localization of fluid flow (e.g. Zhang and Sanderson, 1998, 2001). The widespread development of veins associated with faulting and other forms of deformation attest to past periods of enhanced fluid flow (e.g. Micarelli and Benedicto, 2008). Slip on fractures leads to faults and may produce further localized fracturing (or damage) of the wall rocks (e.g. Kim et al., 2000). The porosity and permeability of the wall rocks may increase due to increased fracture density and/or dilatancy associated with shear on fractures, or may be reduced by the juxtaposition of rocks with differing permeability and the development of fault gouge (e.g. Yielding et al., 1997; Agosta, 2008). Although opening and slip may be viewed as end members, a range of kinematics are developed in faults and fracture zones, with bends and jogs being particularly important in the development of damage and increase of fluid permeability.

We use the term *damage* to describe any type of deformation that is spatially and kinematically associated with a fault or shear zone (e.g. McGrath and Davison, 1995; Kim et al., 2003, 2004; Myers and Aydin, 2004). The term *fault damage zone* has been used with two slightly different meanings in structural geology. One usage is for the *highly deformed zone outside the fault core* (e.g. Shipton and Cowie, 2001, 2003; Billi et al., 2003; Odling et al., 2004; Agosta, 2008), whereas the other usage is for the *zone of secondary structures developed around faults* to accommodate displacement along the fault, especially at fault tips and oversteps (e.g. McGrath and Davison, 1995; Kim et al., 2003, 2004; Flodin and Aydin, 2004; Zhang et al., 2008). In this paper, we mainly use the term with the latter meaning, although wall damage may include aspects of the former.

* Corresponding author. Tel.: +82 51 629 6633; fax: +82 51 629 6623.
E-mail address: ysk7909@pknu.ac.kr (Y.-S. Kim).

0191-8141/$ – see front matter © 2009 Elsevier Ltd. All rights reserved.
doi:10.1016/j.jsg.2009.04.017

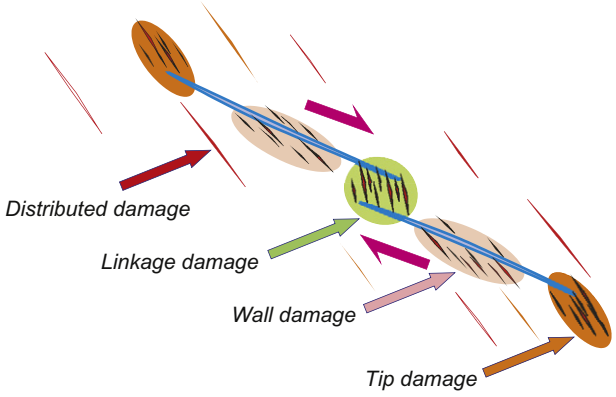

Fig. 1. Classification of damage zones based on location around a segmented fault. *Distributed damage* is scattered extensional fracturing that is formed in the same stress field but prior to the development of the main fault. *Tip damage* is developed in response to stress concentrations and to accommodate changing displacement at the fault tip. *Wall damage* is developed as propagation of tip damage and kinematic damage with accumulating displacement. *Linkage damage* is developed by overprinting of old tips and linking process.

Recent 3-D conceptual damage models around faults (Kim et al., 2003, 2004) provide a basis for the prediction of damage patterns. Fault damage zones are classified into *distributed damage*, *tip damage*, *wall damage,* and *linkage damage* based on the location of fractures around a segmented master fault (Fig. 1; Kim et al., 2004). Damage zones around faults (e.g. McGrath and Davison, 1995; Kim et al., 2003, 2004; Myers and Aydin, 2004) are good targets for exploration of many resources such as groundwater, hydrocarbons, or hydrothermal ore minerals (Li et al., 2001; Micklethwaite and Cox, 2004; Cox and Ruming, 2004; Leckenby et al., 2005; Zhang et al., 2008).

In this paper, we examine the relationship between the density and aperture of fractures and the resulting hydraulic conductance (e.g. Leckenby et al., 2005) or effects of fluid flow (Micklethwaite and Cox, 2004; Cox and Ruming, 2004) based on stalactite distributions in several limestone caves. In particular, the relative amount of fluid flow is quantified in an example of stalactite development in a Korean limestone cave and is related to the location of damage zones around faults.

2. Classification of fault damage

A variety of damage patterns is observed around faults. For simplicity, we will describe mainly those from strike-slip faults. The basic concept of the damage classification and damage patterns is the same for all faults (Kim et al., 2004).

Four types of damage are recognized around a segmented fault (Fig. 1) and can be distinguished based on the location and characteristics of secondary fractures developed in damage zones. The terminology is essentially non-genetic; each of the four categories can result from a range of processes related to the development of the fault, and can be interpreted in terms of the kinematics and dynamics of the fault tip mode and wall rock evolution.

Tip damage (Fig. 1) is developed at the tip of a fault. It is easily recognized, and has been widely reported in the literature (e.g. Segall and Pollard, 1983; Granier, 1985; Pollard and Segall, 1987; McGrath and Davison, 1995; Kim et al., 2003; Micarelli and Benedicto, 2008). This type of damage is developed as a result of stress concentrations and/or to accommodate rapid changes in displacement developed at the fault tip. Tip damage is similar to the *process zone* associated with fracture propagation in crystalline materials, and has been extended to large-scale seismogenic faults (e.g. King, 1986), where it plays an important role in the nucleation and termination of earthquake ruptures. Tip damage has been classified by Kim et al. (2004), and may be easily extended to large-scale faults (e.g. Storti et al., 2003; Kim and Sanderson, 2006). Areas of tensile failure at fault tips are also described from numerical modeling studies (e.g. Bourne and Willemse, 2001; Zhang et al., 2008).

Wall damage occurs where fracturing is distributed within the wall rocks surrounding the fault (Fig. 1), with the degree of fracturing generally decreasing away from the main fault. Various types of wall damage have been recognized that develop by different processes associated with fault growth, and these may be difficult to distinguish. Wall damage is classified into three main categories, including those that form as a result of (a) *mode II tip propagation* (i.e. sequential development of tip damage), (b) the intersection of the *mode III tips* of faults, and (c) increasing strain in the wall rocks due to drag associated with slip on the fault (*kinematic damage*).

Linkage damage (Fig. 1) represents a high intensity of fractures developed between overstepping fault segments (Martel et al., 1988; Peacock and Sanderson, 1991, 1995; Myers and Aydin, 2004). The linkage damage may develop by overprinting of old tip damage zones, or be induced by strain during the evolution of the overstepping fault segments to accommodate accumulating displacement. Linkage damage is classified into two main categories – *dilational* and *contractional jogs*, depending on the sense of stepping in relation to the fault displacement and, hence, the stress conditions in the relay.

We add the term *distributed damage* in this paper to describe fracturing that is more widely distributed in the rock around faults. Such fracturing may occur before the generation of the master fault, and may play a role in the development of the fault and damage zone (e.g. precursory damage of Crider and Peacock, 2004). However, this distributed damage and the wall damage show relatively weak concentration of damage along the fault. Therefore, the main targets for the exploration of resources are tip and linkage damage zones, which will be the main areas of examination and discussion in this paper.

3. 3-D fault damage models

In early models, faults were considered as simple, single planes (e.g. Beckwith, 1941) along which there are displacement gradients

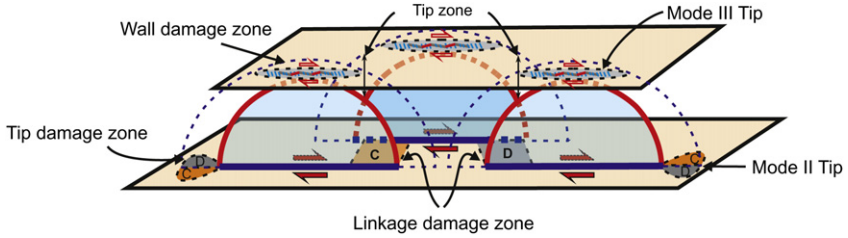

Fig. 2. Simple conceptual 3-D fault damage model showing linkage damage, mode II and mode III tip damages. Wall damage is developed mainly by propagation of mode III tip damage. Some wall damage is developed by propagation of mode II tip and kinematic damage. C indicates contractional zone and D indicates dilational zone.

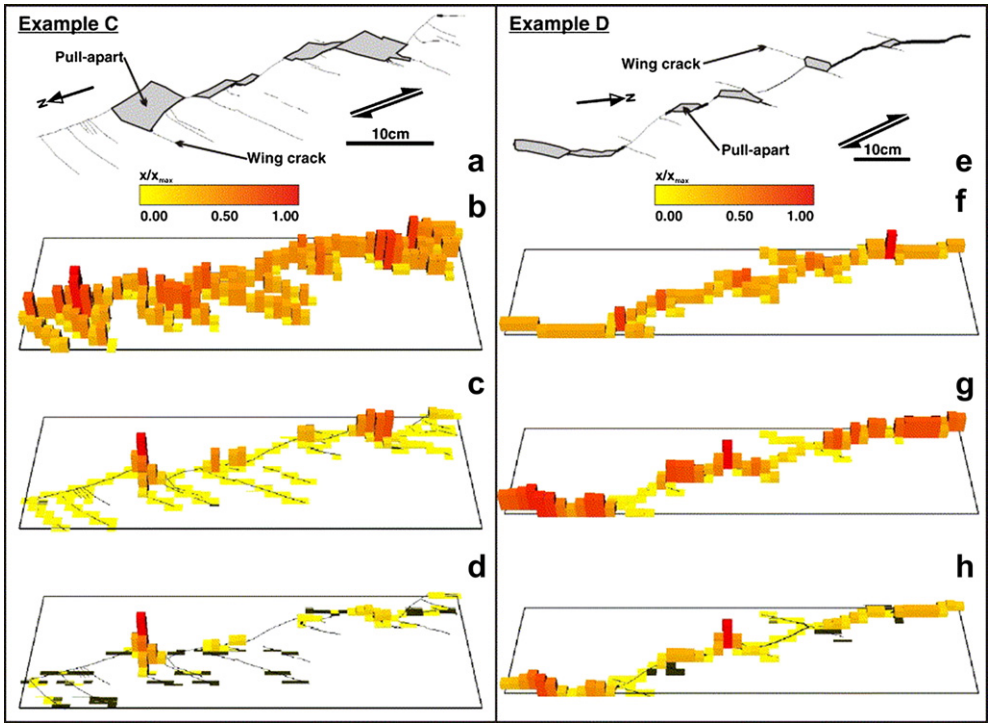

Fig. 3. Examples of dilational steps in strike-slip fault zones. a) and e) Line drawings of veins, shear sense, width and location of relay ramps; line thickness is proportional to vein thickness. The scale bar shows fracture density, fracture aperture and hydraulic conductance normalized to their maximum values. b) and f) Fracture density maps. c) and g) Fracture aperture maps. d) and h) Hydraulic conductance maps (after Leckenby et al., 2005).

from a maximum displacement, generally near the centre, to zero displacement at the tips (Barnett et al., 1987). In the last few decades, faults have been considered as segmented, or bent, irregular planes with complex secondary fracture patterns (e.g. Christie-Blick and Biddle, 1985; Sibson, 1989; Peacock and Sanderson, 1991, 1995). Scholz (1990) illustrated a simple conceptual model for secondary fractures around a fault, based largely on fracture mechanics principles. Martel and Boger (1998) used 3-D boundary element methods to model deformation around a simple, isolated, *penny-shaped* fault, but their model did not explain the variety of secondary fracture patterns around faults (Kim et al., 2004).

Recently, fault damage models have been suggested based on detailed field observation (e.g. McGrath and Davison, 1995; Kim et al., 2003). McGrath and Davison (1995) observed many damage patterns at the lateral and up- or down-dip tips of faults and classified damage patterns around faults based on these observations. This work was extended by Kim et al. (2003), who developed a 3-D model of the damage around a fault and a classification of damage patterns. The basic concept of the 3-D damage models is that the variety of damage patterns results from different fault tip modes and the stage in the evolution of the propagating fault segments or the different location of exposed sections through the master fault (Fig. 2; Kim et al., 2003, 2004).

Two horizontal sections of a segmented strike-slip fault, passing through the centre and top of the fault, can be considered (Fig. 2). If the section is through the centre of the fault, the master fault is seen to be accompanied by linkage damage and tip damage. Mode II tip damage is mainly developed as fractures in the dilational quadrant or ahead of the tip (D at Fig. 2), with pressure solution, thrust faults and folds being developed in contractional quadrants (C at Fig. 2). Intensive linkage damage is developed at the overstep zone, especially at dilational jogs.

On the horizontal section at the top (or bottom) of the fault, a long, narrow zone of distributed tension fractures and secondary shears are predominant along the trend of the master fault (Fig. 2), corresponding to wall damage. This situation is similar to the classical Riedel shear experiments of upward propagation of strike-slip faults (e.g. Riedel, 1929; Tchalenko, 1970; Wilcox et al., 1973). We can equate these classical shear zone models with our mode III tip damage patterns, and models of the damage at the lateral tips of pre-existing discontinuities such as joints (e.g. Segall and Pollard, 1983) with our mode II tip damage patterns. Thus, the 3-D fault damage model can explain almost all the previous fault evolution models. However, sometimes the damage patterns can be modified

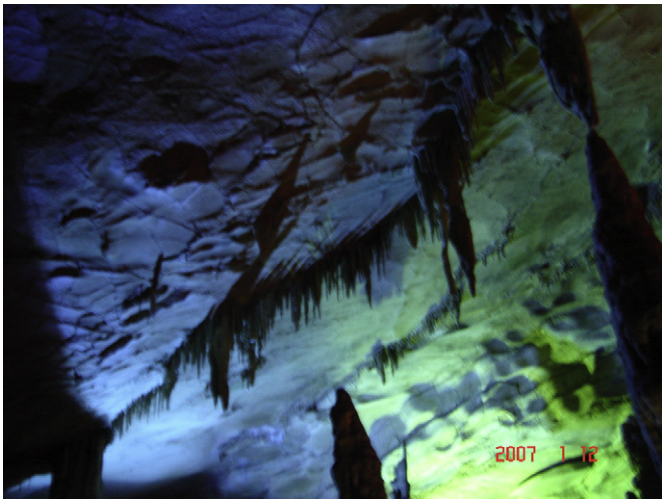

Fig. 4. Examples of stalactites developed along fractures in the Huanglong limestone cave in China. The variation of stalactite sizes indicates relative amounts of fluid flow along the fracture. Bigger and denser stalactites are mainly developed in dilational jogs of the strike-slip faults.

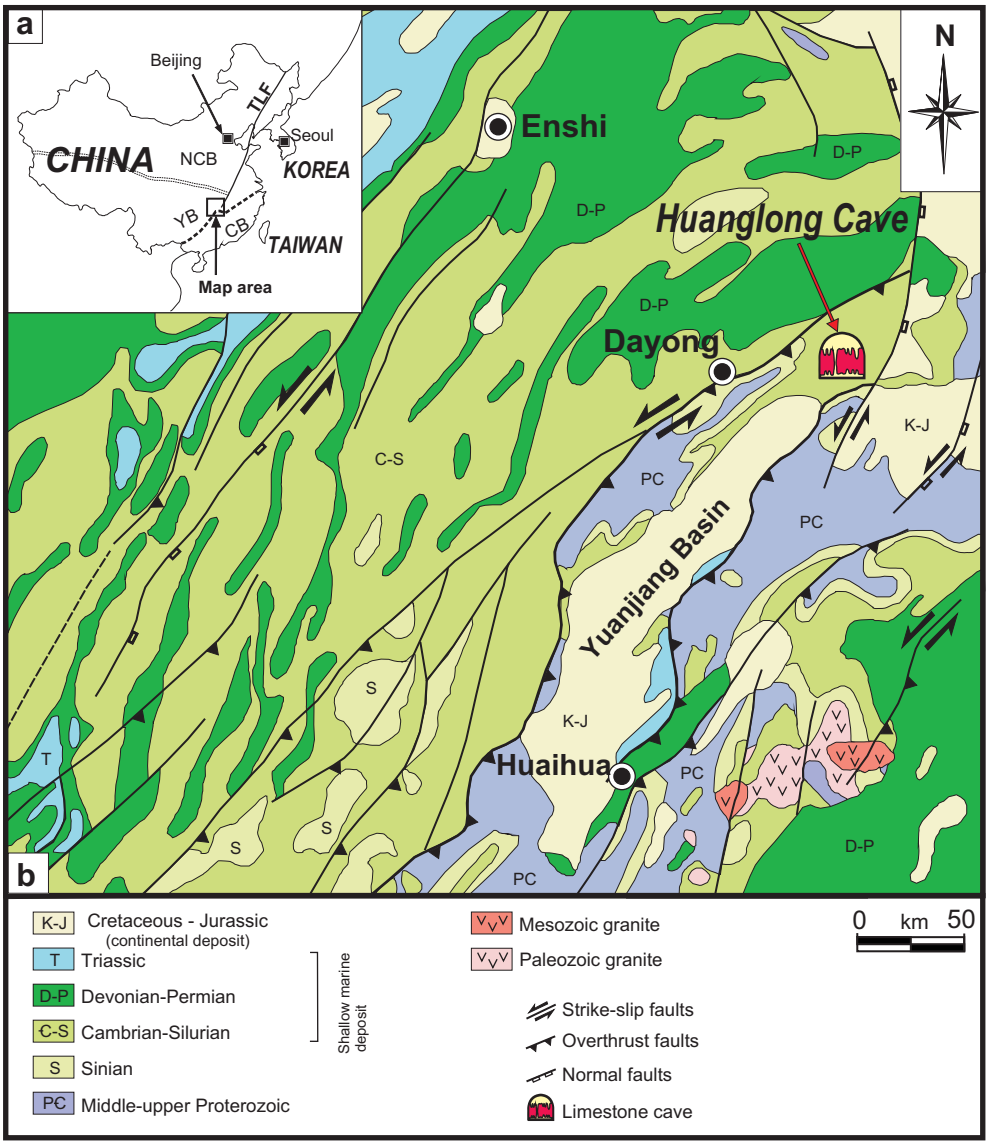

Fig. 5. Location and geological map around the Huanglong cave, Hunan province, China. a) Location map of the study area and main tectonic boundaries between major tectonic units. Abbreviations in the insert: NCB = North China Block, YB = Yangtze Block, CB = Cathaysian Block, TLF = Tan-Lu Fault. b) Geological map around the Huanglong cave (modified from Li et al., 2001; Yan et al., 2003).

depending on tectonic history, material properties (e.g. lithology and ductility), and geometric complexity of master fault surfaces.

4. Linkage damage and fluid flow in dilational jogs

Fluid flow associated with fault damage zones has been discussed by many researchers (e.g. Micklethwaite and Cox, 2004, 2006; Leckenby et al., 2005; Brogi, 2008; Zhang et al., 2008). Leckenby et al. (2005) estimated flow heterogeneity based on fracture density, fracture aperture, and hydraulic conductance. The natural heterogeneity of fracture systems may be caused by several different factors; for example, stress conditions, fracture network connectivity, mineralization, or fluid saturation. They argued that flow localization mainly results from increased fracture aperture and, hence, hydraulic conductance. Different types of fracture patterns display characteristic and predictable patterns of heterogeneity. The conductivity in a fracture network may also change as a function of the orientation and magnitude of the stress system (Sanderson and Zhang, 1999).

The amount of flow should be different in contractional or dilational oversteps. Dilational jogs or pull-aparts show relatively little change in fracture density, but are sites of localized opening and increased conductance (Fig. 3; Leckenby et al., 2005). Contractional jogs may localize fracture, but these are generally closed and of low conductance. Thus, fracture aperture and stepping condition (contractional or dilational) associated with slip sense are very important factors in controlling fluid flow.

4.1. Stalactite examples from limestone caves

It is often very difficult to directly examine the effects of fluid flow within jogs and damage zones. Although we commonly infer the amount of fluid flow from the vein thickness across fractures, final vein thicknesses depend on the history of opening of fractures and precipitation within the fractures. Recently, we found some excellent examples where it is possible to infer the relative amount of fluid flow from stalactites in limestone caves in China

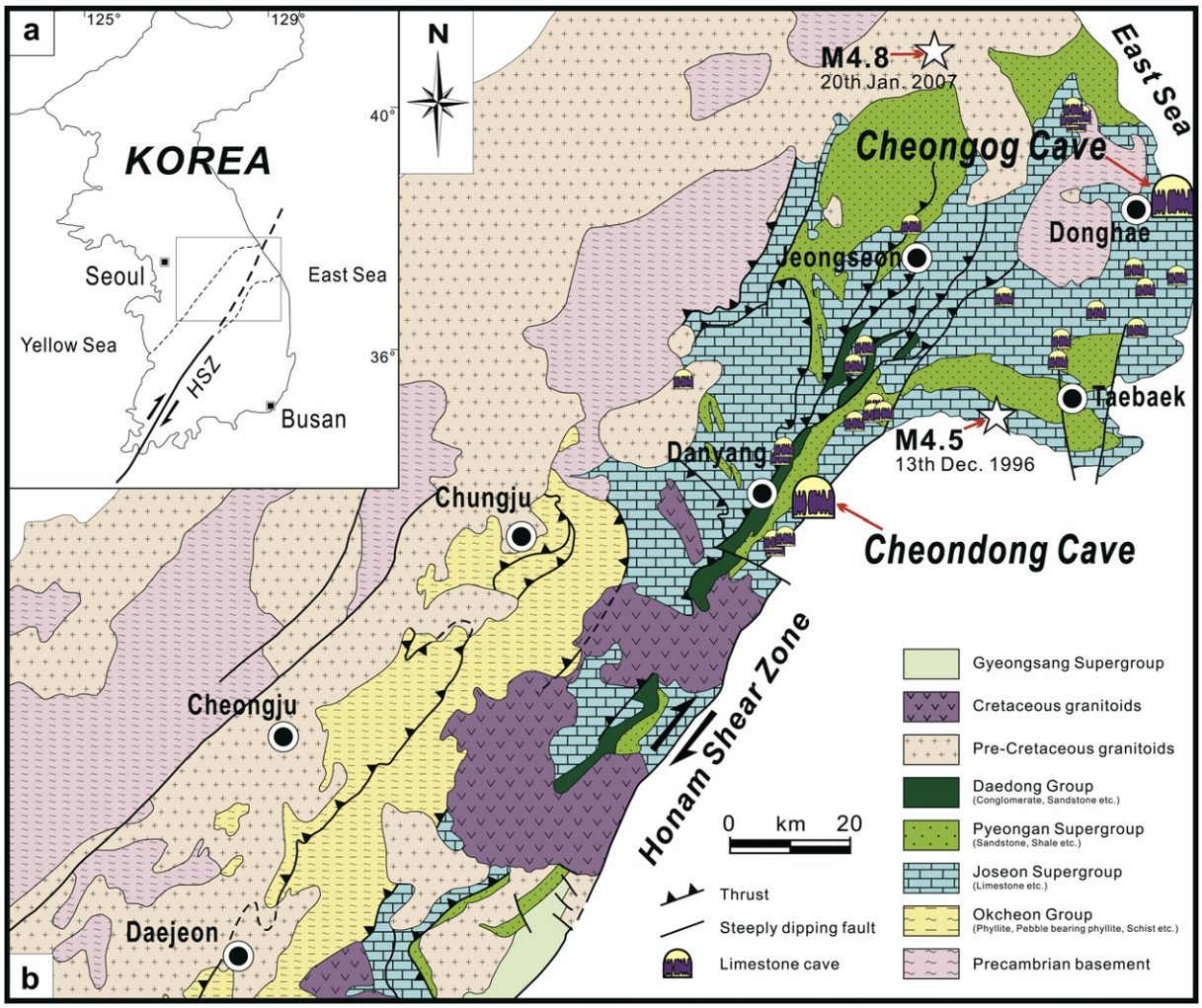

Fig. 6. Geological map of the Okcheon belt (modified from Cluzel et al., 1991; Chough et al., 2000). Thrusts of different ages are not differentiated and have a general NE trend. The Lower Paleozoic Joseon Supergroup is mainly comprised of limestone. Note that most of the limestone caves are developed in the northeastern part of the HSZ. All the reported limestone caves are plotted on the map and the studied Cheondong and Cheongog caves are indicated by bigger symbols.

(Huanglong or Yellow Dragon cave) (Fig. 4) and in South Korea (Chendong and Chengog caves).

In each study area, relationships were observed between the geometry of vertical fractures in the ceiling of caves, and their associated stalactites, with the aim of inferring relative amounts of fluid flow within these fractures. Stalactites and stalagmites are precipitated from acidic underground water that percolates along the faults and fractures dissolving the carbonates. Well developed stalactites along vertical fractures attached on the ceiling of the cave were analyzed to infer the amount of fluid flow. For this

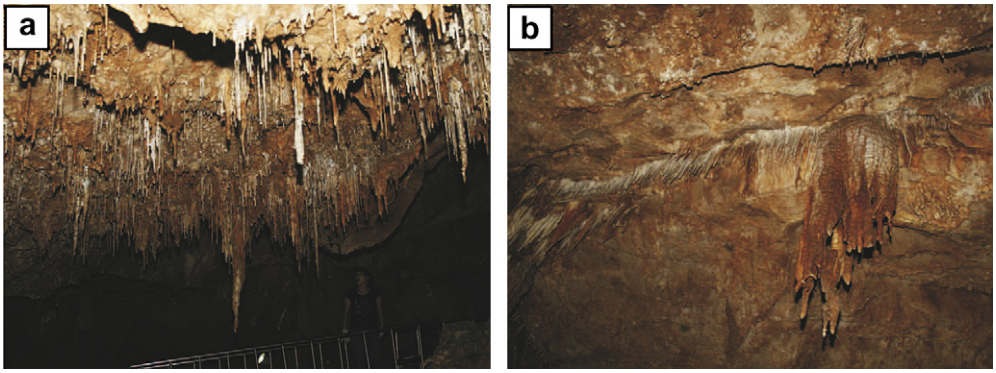

Fig. 7. Influence of fracture density and aperture to stalactite developing patterns. a) Randomly distributed stalactites that are probably controlled by small fracture networks. b) Linearly distributed stalactites. A large stalactite indicates a fluid conduit that is probably controlled by vertical faults. Both are ceiling views in the Cheondong cave.

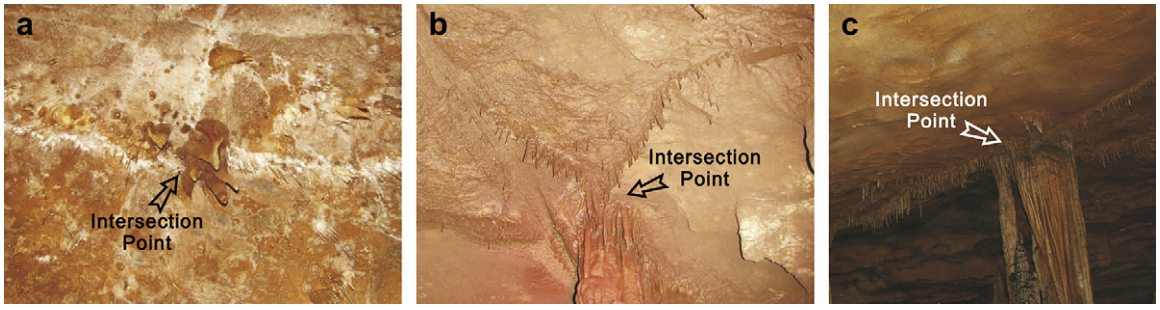

Fig. 8. Influence of fracture intersection to stalactite sizes. Bigger stalactites have been developed where two or more fractures are connected. a) Some large stalactites are developed at an intersection point of two almost perpendicular fractures in the Cheondong cave. b) Several large stalactites are developed at an intersection point of two conjugate type fractures in the Cheongog cave. c) A larger stalactite is developed at a low angle intersection point between two sub-parallel fractures (dilational linkage zone) in the Huanglong cave. All images are ceiling views.

analysis, the sizes of stalactites have been measured, and the distribution patterns of various stalactites are related to the fluid flow characteristics along the fractures.

The Huanglong cave is situated within the Zhangjajie National Forest Park to the east of Dayong city in the northwestern part of the Hunan province, south China (Fig. 5). The park is a very famous tourist attraction due to its spectacularly tall rock columns that form as a result of vertical fractures in the rock. The Huanglong cave area is mainly developed in the Banxi Group of south China (Fig. 5). Sedimentary cover in the Huanglong cave area consists mainly of folded Paleozoic and Lower Mesozoic strata of shallow marine origin (Yan et al., 2003). The cave is one of many limestone caves hosted by Cambrian strata, which comprises black slaty shale, sandstone, and limestone that is interbedded with dolostone.

The Huanglong cave has four layers and covers an area of about 20 km^2. The cave is about 13 km in length, has a vertical height of up to 100 m, and contains a reservoir, two brooks, three waterfalls, four ponds, thirteen halls, and ninety-six passages. The main trend of the Huanlong cave is ENE–WSW.

The major NE-trending compressive deformation structures (thrusts and folds) formed mainly during the Jurassic. Pre-existing normal and thrust faults were reactivated to produce left-lateral strike-slip faults (Li et al., 2001). The study area is located near the tip of the Tan-Lu Fault and may have been partly affected by this major strike-slip fault system. Li et al. (2001) argued that the NNE-trending Hunan–Jiangxi strike-slip fault system, with NE- and NW-trending secondary faults, is still active, generating earthquakes with magnitudes that range from M = 2.0 to 6.0. Stalactites developed along vertical fractures in the ceiling of the cave are probably associated with the fault system (Fig. 4). The average bedding of the limestone in the vicinity of the Huanglong cave dips ~23°NW (strike N72°E). Stalactites that originate from vertical fractures in the ceiling of the cave show very consistent patterns of enhanced fluid flow in dilational jogs (Fig. 4). Unfortunately, the stalactites in this cave were not accessible for direct measurement due to the height of the ceiling.

Several limestone caves are developed in Lower Paleozoic (Cambrian to Ordovician) limestones in Korea. Most of these caves are situated in the northeastern part of the Honam Shear Zone (HSZ; Yanai et al., 1985; Kim and Kee, 1994), a major strike-slip shear zone (Fig. 6), which indicates that the development of the caves may be associated with a right-lateral movement along the shear zone. Two limestone caves (Cheondong and Chengog caves) showed interesting relationships between stalactites and fracture geometries and were selected for this study.

The Cheondong cave is located in the northeastern part of South Korea, about 6 km from the town of Danyang (Fig. 6). The altitude of the Cheondong cave is about 300 m above sea level, and its total length is about 470 m. The main cave is about 200 m long, has an average height of 5–6 m, and trends E–W. The Cheondong cave is hosted by the Lower Paleozoic Dumugol limestone formation, within the Joseon Supergroup of the Okcheon belt.

The Cheongog cave is located near the Donghae city and is located within the Paleozoic Daegi limestone formation (Fig. 6). The N40°W trending Cheongog cave is 30–40 m above sea level and has a total length of about 1400 m. The Daegi limestone formation comprises typically milky white to light gray, massive to thin-bedded limestones, with some oolitic and dolomitic limestones (Cheong, 1969). It has been interpreted to have formed in a shallow marine setting above the wave base (Yun, 1978; Kim and Park, 1981) or in a tidal flat to slope environment (Park and Han, 1986; Park et al., 1987).

A variety of stalactite sizes is developed along vertical fractures associated with small-scale (several meters) strike-slip faults (Figs. 7 and 8). Two basic stalactite patterns occur below the ceiling of the limestone caves; dense clusters of small stalactites along the minor fracture networks (Fig. 7a) and relatively large stalactites that are developed along major faults (Fig. 7b), respectively. This indicates

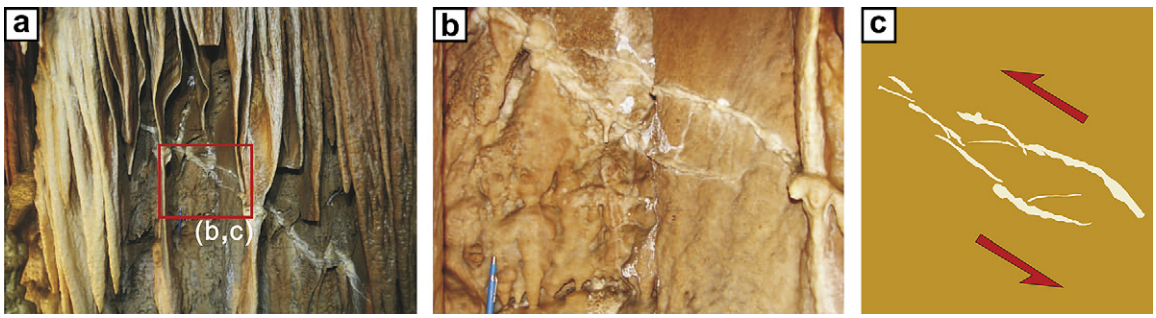

Fig. 9. Evidence for a faulting event controlling late stage stalactite formation in the Cheondong cave. The fault is covered by a later overgrowth of the stalactites. The secondary fracture pattern and fault dip angle indicate a reverse sense of faulting.

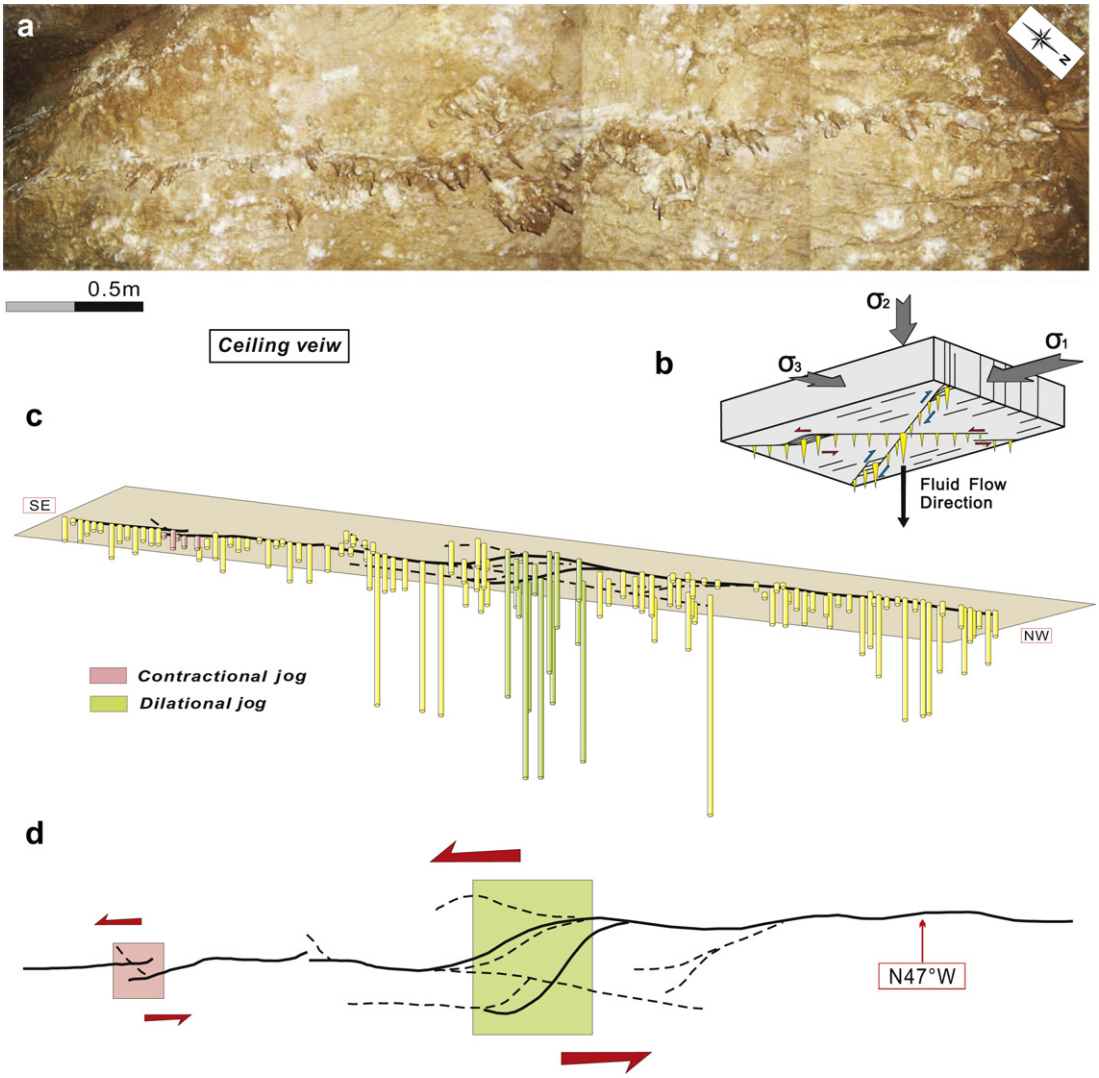

Fig. 10. Examples of a strike-slip fault system and associated stalactites indicating the amount of fluid flow. a) Stalactites hanging from the ceiling of the Cheondong limestone cave in Danyang, Korea. b) Schematic diagram of the fracture patterns, stress conditions, and associated stalactite sizes indicates the amount of fluid flow. c) Line drawing of the fault system and stalactites developed. The length of the cylinder represents the volume of the stalactite (see text for details). d) Contractional jog (red square) and dilational jog (green square) are developed along the strike-slip fault. Larger stalactites occur in the dilational jog, indicating higher fluid flow. The true slip sense of the fault is right-lateral because the view is looking up at the ceiling from the floor of the cave.

that the number of stalactites depends on fracture density, but the size of the stalactites is strongly controlled by fracture aperture. Also, the size of the stalactites is strongly dependant on the positions around fractures, especially in relation to dilational and contractional jogs. Larger and more closely spaced stalactites are mainly developed in dilational jogs (Fig. 4) and intersection points between fractures or faults (Fig. 8).

An interesting structural relationship was noted in the Cheongdong cave. Some of the stalactites are displaced obliquely by a minor fault (Fig. 9), while younger growths of the same stalactites overgrow the fault. These relations indicate that faulting occurred during the growth of the stalactites. Minor thrust faults and en-echelon secondary fractures (R shears and T fractures) along the fault indicate reverse movement. The Danyang area is generally considered to be inactive at present, although some rare medium-scale earthquakes occurred recently near Pyeongchang (M = 4.8, 2007; KMA) and Yeongweol (M = 4.5, 1996; Kyung and Lee, 1996). This structure indicates that the Cheondong cave has experienced at least one seismic event since the start of the stalactite development.

4.2. Quantitative analysis of stalactites

The size of a stalactite is due to both duration and rate of flow through the overlying fractures in the roof of the cave. If the stalactites are of similar age, then their size could be assumed to be proportional to the amount of fluid flow down the almost vertical fractures, parallel to the σ_2 direction (Figs. 4, 10). The relationship is expressed as the following simple equation:

$$Q_{\sigma_2} \propto V_s \tag{1}$$

where Q_{σ_2} is the amount of fluid flow parallel to σ_2 and V_s is the volume of stalactite at each point. For this calculation, it is assumed that other factors affecting stalactite growth are the same at each point. The radius of the circle (r_s) at the top of the stalactite, and the height of the stalactite (h_s) were measured to calculate the stalactite volume (V_s) assuming a conical shape:

$$V_s = 1/3\left(\pi r_s^2 h_s\right) \tag{2}$$

Table 1
Data from 126 stalactites within the Cheondong limestone cave in Danyang, Korea. The radius of the top circle between stalactite and ceiling and the height of stalactite are measured to calculate the volumes of the stalactites. The number of the stalactite is given from the southeast to the northwest (Fig. 10).

Number of stalactite	Radius of stalactite (mm)	Height of stalactite (mm)	Volume of stalactite (mm^3)	Ln (cm)
1	11.5	92	12,734.79	12.73
2	5	61	1596.17	1.60
3	10	99	10,362.00	10.36
4	8.5	81	6125.36	6.13
5	6.5	80	3537.73	3.54
6	7	70	3590.07	3.59
7	12	117	17,634.24	17.63
8	8.5	121	9150.22	9.15
9	8.5	80	6049.73	6.05
10	11	110	13,931.13	13.93
11	7.5	110	6476.25	6.48
12	8.5	112	8469.63	8.47
13	7.5	149	8772.38	8.77
14	4.5	134	2840.13	2.84
15	9	115	9749.70	9.75
16	3.5	131	1679.64	1.68
17	7.5	108	6358.50	6.36
18	7.5	78	4592.25	4.59
19	10	142	14,862.67	14.86
20	5.5	140	4432.63	4.43
21	11.5	131	18,133.24	18.13
22	6.5	74	3272.40	3.72
23	5	91	2381.17	2.38
24	7.5	85	5004.38	5.00
25	3.5	40	512.87	0.51
26	11	125	15,830.83	15.83
27	3.5	42	538.51	0.54
28	3.5	41	525.69	0.53
29	12	135	20,347.20	20.35
30	9	103	8732.34	8.73
31	11.5	130	17,994.82	17.99
32	7	79	4051.65	4.05
33	10.5	119	13,732.01	13.73
34	7	80	4102.93	4.10
35	7.5	86	5063.25	5.06
36	5	61	1596.17	1.60
37	5	57	1491.50	1.49
38	8	92	6162.77	6.16
39	7.5	85	5004.38	5.00
40	12	138	20,799.36	20.80
41	16.5	168	47,872.44	47.87
42	21	173	79,853.34	79.85
43	12	137	20,648.64	20.65
44	11.5	131	18,133.24	18.13
45	11.5	135	18,686.93	18.69
46	11	129	16,337.42	16.34
47	11.5	131	18,133.24	18.13
48	21	182	84,007.56	84.01
49	14	139	28,515.39	28.52
50	21.5	176	85,152.61	85.15
51	19.5	201	79,997.00	80.00
52	10.5	120	13,847.40	13.85
53	22.5	226	11,9751.75	119.75
54	7.5	86	5063.25	5.06
55	10	123	12,874.00	12.87
56	15	171	40,270.50	40.27
57	12.5	137	22,405.21	22.41
58	19.5	212	84,374.94	84.37
59	10	118	12,350.67	12.35
60	13	148	26,179.23	26.18
61	10	119	12,455.33	12.46
62	10.5	125	14,424.38	14.42
63	23.5	193	11,1558.18	111.56
64	10.5	118	13,616.61	13.62
65	10.5	124	14,308.98	14.31
66	11.5	135	18,686.93	18.69
67	23	202	11,1844.71	111.84
68	21	169	78,007.02	78.01
69	15.5	137	34,450.25	34.45
70	13	138	24,410.36	24.41
71	15	161	37,915.50	37.92
72	10.5	125	14,424.38	14.42
73	10.5	126	14,539.77	14.54
74	12.5	132	21,587.50	21.59
75	11	125	15,830.83	15.83
76	13.5	153	29,185.52	29.19
77	7	80	4102.93	4.10
78	11	125	15,830.83	15.83
79	6	72	2712.96	2.71
80	11	124	15,704.19	15.70
81	5	59	1543.83	1.54
82	10	115	12,036.97	12.04
83	5.5	69	2184.66	2.18
84	10.5	125	14,424.38	14.42
85	12.5	139	22,732.29	22.73
86	14	159	32,618.32	32.62
87	10	114	11,932.00	11.93
88	6.5	74	3272.40	3.27
89	24	213	12,8413.44	128.41
90	10	111	11,618.00	11.62
91	6.5	74	3272.40	3.27
92	5.5	66	2089.67	2.09
93	12.5	129	21,096.88	21.10
94	6	72	2712.96	2.71
95	11	123	15,577.54	15.58
96	10	114	11,932.00	11.93
97	6.5	77	3405.07	3.41
98	11.5	131	18,133.24	18.13
99	9.5	110	10,390.78	10.39
100	8.5	98	7410.92	7.41
101	12	129	19,442.88	19.44
102	10	109	11,408.67	11.40
103	6	70	2637.60	2.64
104	9	103	8732.34	8.73
105	15	141	33,205.50	33.21
106	15	149	35,089.50	35.09
107	16.5	168	47,872.44	47.87
108	6.5	74	3272.40	3.27
109	7.5	85	5004.38	5.00
110	6.5	74	3272.40	3.27
111	19.5	174	69,251.13	69.25
112	11	125	15,830.83	15.83
113	6.5	74	3272.40	3.27
114	18.5	190	68,062.12	68.06
115	18	185	62,737.20	62.74
116	10.5	125	14,424.38	14.42
117	8.5	96	7259.68	7.26
118	11.5	129	17,856.40	17.86
119	15.5	156	39,228.02	39.23
120	12.5	142	23,222.92	23.22
121	15.5	166	41,742.64	41.74
122	10.5	125	14,424.38	14.42
123	11.5	129	17,856.40	17.86
124	9	103	8732.34	8.73
125	14.5	135	29,708.33	29.71
126	10.5	125	14,424.38	14.42

The stalactites and related stress and fracture system from a small cave at Danyang in Korea are shown in Fig. 10, and the calculated volumes of all stalactites are listed in Table 1. The plot of the stalactites (Fig. 10c) shows their size as a cylinder with a base of unit area. Thus the heights (L_n) of the cylinders represent the volume of the stalactites rather than their measured length, where the volume (V_n) for an arbitrary stalactite can be expressed as follows:

$$V_n = 1/3\left(\pi r_n^2 h_n\right) = A_u L_n \quad (3)$$

where r_n is the radius of an arbitrary circle between stalactite and ceiling, h_n is the height of the stalactite and L_n is the length of cylinder of equivalent volume, having a circular area A_u.

The fault system in the Cheondong cave includes both dilational and contractional jogs and provides a good example for the comparison of relationships in two different locations (Fig. 10c, d). The distribution and volume of the stalactites at contractional and dilational jogs are clearly distinguished (Table 1 and Fig. 10c). In the contractional jog, the stalactites are relatively small and rare, although the overlapping area is relatively small and less clear than for the dilational jog. On the other hand, the stalactites in the dilational jog are much bigger than those in the contractional jog, which indicates an enhanced fluid flow.

Although we could not measure the length of the stalactites in the Huanglong cave, China, many similar patterns also occur (Figs.4 and 8c). In general, the flow along the main segments is intermediate between the two types of jog, but high flows may occur locally in more dilational parts of the faults. Thus, stalactites hanging below the ceilings of limestone caves are good indicators of vertical fluid flow (parallel to σ_2 direction) along strike-slip faults. They indicate that fluid flow, in addition to intersection points of fractures, is strongly controlled by kinematic locations (either contractional or dilational) and slip senses (either right-lateral or left-lateral) along the fault system.

5. Discussion

5.1. Damage zones and mineralization

Deep faults, and their associated structures within strike-slip regimes, may have acted as pumping systems in the transport of fluid from deeper crustal levels to shallower levels (Sibson, 1987). On the other hand, surface fluids including meteoric water, groundwater and formation water, could percolate downward along the fault zones. These fluids can mix around the seismic–aseismic transition zone (10–15 km; Sibson et al., 1975) and then migrate upwards.

For example, in South China over 100 modern hot springs lie along the Hunan–Jiangxi strike-slip fault system (Li et al., 2001), which is one of the largest spring concentrations in China. They reflect a major thermal anomaly and groundwater outflow in the area, which are probably controlled by the activity of the fault system. A similar phenomenon is observed in the distribution of limestone caves in Korea. The limestone caves are mainly developed in the dilational quadrant of a major strike-slip shear zone (Fig. 6).

Mineral deposits commonly form as a result of direct precipitation of hydrothermal solutions or through fluid–rock interaction. The spatial variation of mineralization within a fault zone essentially shows the relation between fault movement, fluid flow, and subsequent ore deposition. Field investigations and analogue experiments (Cox, 1999) have shown that fluid flow is localized where permeability is highest (Leckenby et al., 2005). These locations are basically dilational and have governed the localization and geometry of the deposits, as demonstrated by studies of vein gold system of Martha Hill, New Zealand (Sibson, 1987), the Mesquite mining district, SE California (Willis and Tosdal, 1992), and the giant Golden Mile ore system in the Kalgoorlie–Kambalda area, Western Australia (Cox, 1999). Uranium deposits from South China provide additional spectacular examples of the importance of dilational segments along strike-slip fault zones for localizing fluids and controlling deposit geometry (Li et al., 2001).

Pull-apart stepovers, dilational fault tips, local releasing bends, extensional linkage zones and fault intersections are the most favorable sites for fluid circulation because of the intense opening and high permeability within these zones. From this point of view, dilational damage zones have played important roles in the formation and distribution of hydrothermal deposits (e.g. Willis and Tosdal, 1992; Cox, 1999; Li et al., 2001) and igneous intrusions (e.g. Hutton et al., 1990). Fig. 11 illustrates the effect of pull-apart stepovers on the formation and distribution of uranium deposits in the Lujing orefield, one of the largest uranium orefields in China (Li et al., 2001).

Another potential site for mineralization is in the dilational tip damage zones of faults. Simple strike-slip faults, at a wide range of scales, consist of two basic parts: the central linear trace and various tip-structures (Kim and Sanderson, 2006). These are sites for mineralized breccias, stockworks, and vein sets that generally show combinations of extension and shear. Therefore, the dilational tip damage zone acts as the possible site for magma emplacement, hydrothermal activity, and related mineralization (Cox, 1999).

5.2. Seismogenic controls on fluid flow

For the majority of seismic events, the jog zone would be a common site for rupture termination, dilation, and enhanced fluid flow (Sibson, 1987). Structures adjacent to the jog are relatively immature, low--displacement fault and vein networks, and could act as localized channels for high-flux fluid flow (Micklethwaite and Cox, 2004).

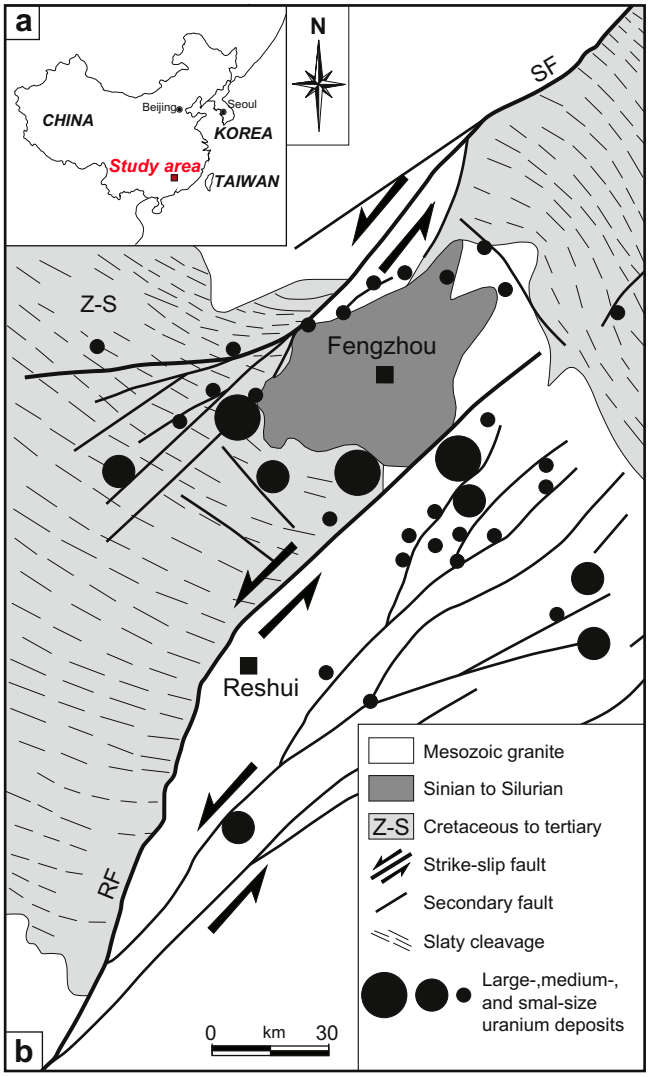

Fig. 11. Geological map and location of the Lujing uranium orefield near strike-slip faults. The most important uranium deposits are located within the stepover between the Suichuan Fault (SF) and the Reshui Fault (RF) (modified from Li et al., 2001).

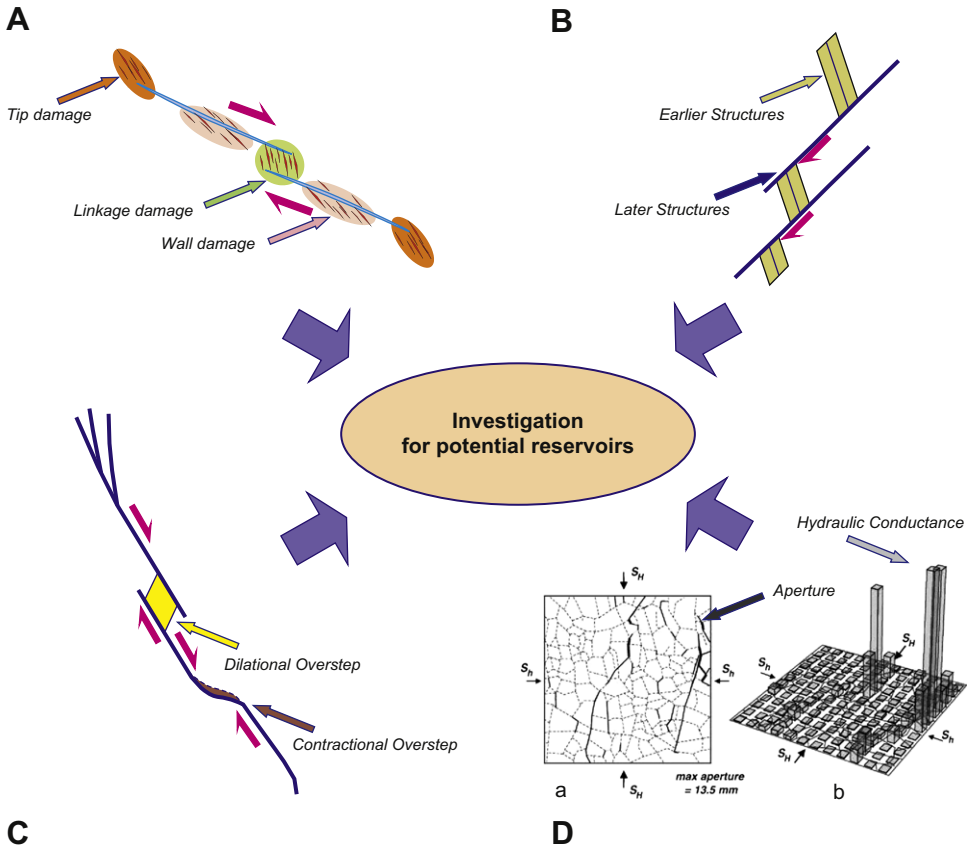

Fig. 12. Stages in the interpretation of ancient flow systems in reservoirs associated with faults and damages. (A) Geometrical analysis of faults and damage zones; (B) Establishing deformation history; (C) Kinematic analysis of fractures; (D) Evaluation of conductivity of fractures.

During and shortly after rupture, both the ruptured fault zone and the aftershock zone are sites with enhanced permeability. However, more protracted fluid flow is likely to occur in the aftershock zones. In contrast, on the main rupture surface, porosity is created over a broad area but may not be maintained. Rapid sealing of the fluid pathways occurs by compaction and precipitation of minerals (e.g. Tenthorey et al., 2003). Therefore, rupture on the main fault leads to elevated fluid flux through the aftershock structures over a protracted period, but through the main structure for only a short period (Micklethwaite and Cox, 2004). Thus, contractional jogs or bends on large faults are just as likely to lead to transiently permeable zones of crust as a dilational jog (e.g. Cox and Ruming, 2004).

5.3. Fracture-controlled fluid flow in ancient systems

It is important to remember that veins and mineral deposits indicate paleo-fluid systems through fractures, and only provide indirect evidence for fluid flow around fault systems. Furthermore, old fractures may be sealed by later hydrothermal or magmatic activity; hence, their present-day role in controlling fluid flow may be very different from that in the past.

Stalactites are used to quantify the amount of fluid flow and the fluid flow characteristics in carbonate rocks. Although it is assumed that other factors affecting stalactite growth are the same at each point, they should be carefully investigated for more reliable interpretation and detailed study. Other controlling factors that should be considered include fluid pathways, regional tectonic setting, history of the fault, local fault structure, fault activity, depth of the cave, underground level, surface drainage patterns, fault type, aperture, and bedding dips.

To interpret fracture-controlled fluid flow in ancient systems it is necessary to approach the problem carefully. The first step is to characterize the geometry of the faults and fractures, paying particular attention to the nature and origin of damage zones and their location around faults (Fig. 12A). The next step is to evaluate the deformation history of the area, in order to relate different elements of the structure to one another (Fig. 12B). For this step, it is important to identify both structural and fluid flow events. It is then necessary to establish the kinematics of the structures during each deformation event (Fig. 12C), because the geometrical elements may have very different controls under different kinematic regimes. Finally, it is necessary to assess how the conductivity (permeability) might be affected by the different structures at varying times and under varying kinematic regimes (Fig. 12D).

6. Conclusions

Damage zones are regions of deformation around faults, which are mainly classified based on their location. Fluid flow around faults is mainly controlled by the master fault, associated damage zones and stress conditions.

The analysis of stalactites and controlling fault systems in limestone caves from China and Korea demonstrates that fluid flow and related mineralization are influenced by the fault-related fractures and their kinematics. Although both fracture density and aperture control hydraulic conductance, fracture density has minimal influence on the associated fluid flow. Dilation or opening along fractures is the main control on the fluid flux. In this study,

we use stalactites developed in limestone caves to demonstrate fluid flow localization on master faults and in dilational damage zones. The distribution of stalactite size is strongly controlled by the kinematic locations and movement sense along the fault. In contractional jogs the stalactites are relatively small and rare, whereas in the dilational jog they are much bigger and more numerous. The size and density of the stalactites provide a direct measure of fluid flow and are strongly controlled by linkage damage patterns and intersection of fractures.

This study provides a field-based method for comparing fluid flow in fault systems, which is an alternative to numerical and laboratory studies. In the future, additional data, such as the dating of carbonate concretions and their isotope signatures, may provide important insights into the activity of related faults and the circulation of fluids that feed the carbonate concretions.

Acknowledgement

This work was supported by the Korea Research Foundation Grant funded by the Korean Government (MOEHRD) (KRF-2006-331-C00286). We thank Kwangmin Jin, Seung-Rok Han, and Jin-Hyeuk Choi for their fieldwork and data analysis. Fabrizio Agosta, Andrea Billi, Paul Duuring and an anonymous reviewer are thanked for their very constructive reviews and comments, which greatly improved this paper.

References

Agosta, F., 2008. Fluid flow properties of basin-bounding normal faults in platform carbonates, Fucino Basin, central Italy. In: Wibberley, C.A.J., Kurz, W., Imber, J., Holdsworth, R.E., Collettini, C. (Eds.), The Internal Structure of Fault Zones: Implications for Mechanical and Fluid-flow Properties. Geological Society, London, Special Publications, vol. 299, pp. 277–291.

Barnett, J.A.M., Mortimer, J., Rippon, J.H., Walsh, J.J., Watterson, J., 1987. Displacement geometry in the volume containing a single normal fault. American Association of Petroleum Geologists Bulletin 71, 925–937.

Beckwith, R.H., 1941. Trace-slip faults. American Association of Petroleum Geologists Bulletin 25, 2181–2193.

Billi, A., Salvini, F., Storti, F., 2003. The damage zone-fault core transition in carbonate rocks: implications for fault growth, structure and permeability. Journal of Structural Geology 25, 1779–1794.

Bourne, S.J., Willemse, E.J.M., 2001. Elastic stress control on the pattern of tensile fracturing around a small fault network at Nash Point, UK. Journal of Structural Geology 23, 1753–1770.

Brogi, A., 2008. Fault zone architecture and permeability features in siliceous sedimentary rocks: insights from the Rapolano geothermal area (Northern Apennines, Italy). Journal of Structural Geology 30, 237–256.

Cheong, C.H., 1969. Stratigraphy and paleontology of the Samcheog coalfield, Gangweondo, Korea (1). Journal of the Geological Society of Korea 5, 13–56 (in Korean with English abstract).

Chough, S.K., Kwon, S.-T., Ree, J.-H., Choi, D.K., 2000. Tectonic and sedimentary evolution of the Korean peninsula: a review and new view. Earth Science Reviews 52, 175–235.

Christie-Blick, N., Biddle, K.T., 1985. Deformation and basin formation along strike-slip faults. In: Biddle, K.T., Christie-Blick, N. (Eds.), Strike-slip Deformation, Basin Formation, and Sedimentation. Society of Economic Palaeontologists and Mineralogists, Special Publications, vol. 37, pp. 1–34.

Cluzel, D., Lee, B.-J., Cadet, J.-P., 1991. Indosinian dextral ductile fault system and synkinematic plutonism in the southwest of the Ogcheon belt (South Korea). Tectonophysics 194, 131–151.

Cox, S.F., 1999. Deformation controls on the dynamics of fluid flow in mesothermal gold systems. In: McCafferey, K., Lonergan, L., Wilkinson, J. (Eds.), Fracture, Fluid Flow and Mineralization. Geological Society, London, Special Publications, vol. 155, pp. 123–140.

Cox, S.F., Ruming, K., 2004. The St. Ives mesothermal gold system, Western Australia – a case of golden aftershocks? Journal of Structural Geology 26, 1109–1125.

Crider, J.G., Peacock, D.C.P., 2004. Initiation of brittle faults in the upper crust: a review of field observations. Journal of Structural Geology 26, 691–707.

Flodin, E., Aydin, A., 2004. Faults with asymmetric damage zones in sandstone, Valley of Fire State Park, southern Nevada. Journal of Structural Geology 26, 983–988.

Granier, T., 1985. Origin, damping, and pattern of development of faults in granite. Tectonics 4, 721–737.

Hutton, D.H.W., Dempster, T.T., Brown, P.E., 1990. A new mechanism of granite emplacement: intrusion in active extensional shear zones. Nature 334, 452–455.

Kim, J.H., Kee, W.-S., 1994. Structural characteristics of the Soonchang shear zone, Korea. Journal of Southeast Asian Earth Sciences 9, 417–428.

Kim, J.Y., Park, Y.A., 1981. Sedimentological study of the Pungchon and Hwajeol Formations, Gangweon-do, Korea. Journal of the Geological Society of Korea 17, 225–240 (in Korean with English abstract).

Kim, Y.-S., Andrews, J.R., Sanderson, D.J., 2000. Damage zones around strike-slip fault systems and strike-slip fault evolution, Crackington Haven. Southwest England Geosciences Journal 4, 53–72.

Kim, Y.-S., Peacock, D.C.P., Sanderson, D.J., 2003. Mesoscale strike-slip faults and damage zones at Marsalforn, Gozo Island, Malta. Journal of Structural Geology 25, 793–812.

Kim, Y.-S., Peacock, D.C.P., Sanderson, D.J., 2004. Fault damage zones. Journal of Structural Geology 26, 503–517.

Kim, Y.-S., Sanderson, D.J., 2006. Structural similarity and variety at the tips in a wide range of strike-slip faults: a review. Terra Nova 18, 330–344.

King, G.C.P., 1986. Speculations on the geometry of the initiation and termination processes of earthquake rupture and its relation to morphology and geological structure. Pure and Applied Geophysics 124, 567–585.

KMA (Korea Meteorological Administration) http://www.kma.go.kr.

Kyung, J.B., Lee, K., 1996. Analysis on the damage and intensity of the 13 December 1996 Yeongweol earthquake. The Journal of Engineering Geology 6, 165–184 (in Korean with English abstract).

Leckenby, R.J., Sanderson, D.J., Lonergan, L., 2005. Estimating flow heterogeneity in natural fracture systems. Journal of Volcanology and Geothermal Research 148, 116–129.

Li, J.W., Zhou, M.F., Li, X.F., Fu, Z.R., Li, Z.J., 2001. The Hunan–Jiangxi strike-slip fault system in South China: southern extension of the Tan-Lu fault. Journal of Geodynamics 32, 333–354.

Martel, S.J., Boger, W.A., 1998. Geometry and mechanics of secondary fracturing around small three-dimensional faults in granitic rock. Journal of Geophysical Research 103, 21299–21314.

Martel, S.J., Pollard, D.D., Segall, P., 1988. Development of simple strike-slip fault zones, Mount Abbot quadrangle, Sierra Nevada, California. Geological Society of America Bulletin 100, 1451–1465.

McGrath, A.G., Davison, I., 1995. Damage zone geometry around fault tips. Journal of Structural Geology 17, 1011–1024.

Micarelli, L., Benedicto, A., 2008. Normal fault terminations in limestones from the SE-Basin (France): implications for fluid flow. In: Wibberley, C.A.J., Kurz, W., Imber, J., Holdsworth, R.E., Collettini, C. (Eds.), The Internal Structure of Fault Zones: Implications for Mechanical and Fluid-flow Properties. Geological Society, London, Special Publications, vol. 299, pp. 123–138.

Micklethwaite, S., Cox, S.F., 2004. Fault-segment rupture, aftershock-zone fluid flow, and mineralization. Geology 32, 813–816.

Micklethwaite, S., Cox, S.F., 2006. Progressive fault triggering and fluid flow in aftershock domains: examples from mineralized Archaean fault systems. Earth and Planetary Science Letters 250, 318–330.

Myers, R., Aydin, A., 2004. The evolution of faults formed by shearing across joint zones in sandstone. Journal of Structural Geology 26, 947–966.

Odling, N.E., Harris, S.D., Knipe, R.J., 2004. Permeability scaling properties of fault damage zones in siliclastic rocks. Journal of Structural Geology 26, 1727–1747.

Park, B.K., Han, J.H., Han, S.J., 1987. Cambrian peritidal mudstone deposits interbedded in the Pungchon Limestone Formation, Korea. Journal of the Geological Society of Korea 23, 60–66 (in Korean with English abstract).

Park, B.K., Han, S.J., 1986. Middle Cambrian ooid shoal deposits: the oolitic carbonate rocks of Lower Punchon Limestone Formation, Korea. Journal of the Geological Society of Korea 22, 183–199 (in Korean with English abstract).

Peacock, D.C.P., Sanderson, D.J., 1991. Displacement and segment linkage and relay ramps in normal fault zones. Journal of Structural Geology 13, 721–733.

Peacock, D.C.P., Sanderson, D.J., 1995. Pull-aparts, shear fractures and pressure solution. Tectonophysics 241, 1–13.

Pollard, D.D., Segall, P., 1987. Theoretical displacements and stresses near fractures in rock: with applications to faults, joints, veins, dikes, and solution surfaces. In: Atkinson, B.K. (Ed.), Fracture Mechanics of Rock. Academic Press, London, pp. 277–349.

Riedel, W., 1929. Zur Mechanik geologischer Brucherscheinungen. Zentralblatt für Mineralogie, Geologie, and Palaeontologie 1929B, 354–368.

Sanderson, D.J., Zhang, X., 1999. Critical stress localization of flow associated with deformation of well-fractured rock masses, with implications for mineral deposits. In: McCaffrey, K.J.W., Lonergan, L., Wilkinson, J.J. (Eds.), Fractures, Fluid Flow and Mineralisation. Geological Society, London, Special Publications, vol. 155, pp. 69–81.

Scholz, C.H., 1990. The Mechanics of Earthquakes and Faulting. Cambridge University Press, Cambridge, p. 439.

Segall, P., Pollard, D.D., 1983. Nucleation and growth of strike-slip faults in granite. Journal of Geophysical Research 88, 555–568.

Shipton, Z.K., Cowie, P.A., 2001. Damage zone and slip-surface evolution over μm to km scales in high-porosity Navajo sandstone, Utah. Journal of Structural Geology 23, 1825–1844.

Shipton, Z.K., Cowie, P.A., 2003. A conceptual model for the origin of fault damage zone structures in high-porosity sandstone. Journal of Structural Geology 25, 333–344.

Sibson, R.H., Moore, J.M.C., Rankin, A.H., 1975. Seismic pumping - A hydrothermal fluid transport mechanism. Journal of Geological Society of London 131, 653–659.

Sibson, R.H., 1987. Earthquake rupturing as a mineralizing agent in hydrothermal systems. Geology 15, 701–704.

Sibson, R.H., 1989. Earthquake faulting as a structural process. Journal of Structural Geology 11, 1–14.

Storti, F., Holdsworth, R.E., Salvini, F., 2003. Intraplate strike-slip deformation belts. In: Storti, F., Holdsworth, R.E., Salvini, F. (Eds.), Intraplate Strike-slip Deformation Belts. Geological Society, London, Special Publications, vol. 210, pp. 1–14.

Tchalenko, J.S., 1970. Similarities between shear zones of different magnitudes. Geological Society of America Bulletin 81, 1625–1640.

Tenthorey, E., Cox, S.F., Todd, H.F., 2003. Evolution of strength recovery and permeability during fluid–rock reaction in experimental fault zones. Earth and Planetary Science Letters 206, 161–172.

Wilcox, R.E., Harding, T.P., Seely, D.R., 1973. Basic wrench tectonics. American Association of Petroleum Geologists Bulletin 57, 74–96.

Willis, G.F., Tosdal, R.M., 1992. Formation of gold veins and breccias during dextral strike-slip faulting in the Mesquite mine district, southeastern California. Economic Geology 87, 2002–2022.

Yan, D.P., Zhou, M.F., Song, H.L., Wang, X.W., Malpas, J., 2003. Origin and tectonic significance of a Mesozoic multi-layer over-thrust system within the Yangtze Block (South China). Tectonophysics 361, 239–254.

Yanai, S., Park, B.S., Otoh, S., 1985. The Honam shear zone (South Korea): deformation and tectonic implication in the Far East. Scientific Papers of the College of Arts and Sciences, University of Tokyo 35, 181–210.

Yielding, G., Freeman, B., Needham, D.T., 1997. Quantitative fault-seal prediction. American Association of Petroleum Geologists Bulletin 81, 897–917.

Yun, S., 1978. Petrology, chemical composition, and depositional environments of the Cambro-Ordovician sedimentary sequences in the Yeonhwa I Mine area, southeastern Taebaegsan region, Korea. Journal of the Geological Society of Korea 14, 145–174 (in Korean with English abstract).

Zhang, X., Sanderson, D.J., 1998. Numerical study of critical behaviour of deformation and permeability of fractured rock masses. Marine and Petroleum Geology 15, 535–548.

Zhang, X., Sanderson, D.J., 2001. Evaluation of instability in fractured rock masses using numerical analysis methods: effects of fracture geometry and loading direction. Journal of Geophysical Research 106, 26671–26687.

Zhang, Y., Schaubs, P.M., Zhao, C., Ord, A., Hobbs, B.E., Barnicoat, A.C., 2008. Fault-related dilation, permeability enhancement, fluid flow and mineral precipitation patterns: numerical models. In: Wibberley, C.A.J., Kurz, W., Imber, J., Holdsworth, R.E., Collettini, C. (Eds.), The Internal Structure of Fault Zones: Implications for Mechanical and Fluid-flow Properties. Geological Society, London, Special Publications, vol. 299, pp. 239–255.